J Pharmacokinet Pharmacodyn (2015) 42:639–657
DOI 10.1007/s10928-015-9430-4

ORIGINAL PAPER

Application of a Bayesian approach to physiological modelling of mavoglurant population pharmacokinetics

Thierry Wendling[1,2] · Swati Dumitras[2] · Kayode Ogungbenro[1] · Leon Aarons[1]

Received: 9 June 2015 / Accepted: 27 July 2015 / Published online: 1 August 2015

Abstract Mavoglurant (MVG) is an antagonist at the metabotropic glutamate receptor-5 currently under clinical development at Novartis Pharma AG for the treatment of central nervous system diseases. The aim of this study was to develop and optimise a population whole-body physiologically-based pharmacokinetic (WBPBPK) model for MVG, to predict the impact of drug–drug interaction (DDI) and age on its pharmacokinetics. In a first step, the model was fitted to intravenous (IV) data from a clinical study in adults using a Bayesian approach. In a second step, the optimised model was used together with a mechanistic absorption model for exploratory Monte Carlo simulations. The ability of the model to predict MVG pharmacokinetics when orally co-administered with ketoconazole in adults or administered alone in 3–11 year-old children was evaluated using data from three other clinical studies. The population model provided a good description of both the median trend and variability in MVG plasma pharmacokinetics following IV administration in adults. The Bayesian approach offered a continuous flow of information from pre-clinical to clinical studies. Prediction of the DDI with ketoconazole was consistent with the results of a non-compartmental analysis of the clinical data (threefold increase in systemic exposure). Scaling of the WBPBPK model allowed reasonable extrapolation of MVG pharmacokinetics from adults to children. The model can be used to predict plasma and brain (target site) concentration–time profiles following oral administration of various immediate-release formulations of MVG alone or when co-administered with other drugs, in adults as well as in children.

Keywords Mavoglurant · Population pharmacokinetics · Physiologically-based pharmacokinetic models · Bayesian analysis · Drug–drug interactions · Paediatrics

Introduction

Mavoglurant (MVG) is an antagonist at the metabotropic glutamate receptor 5 currently under clinical development at Novartis Pharma AG for the treatment of central nervous system diseases. Although MVG can be administered by both the intravenous (IV) and oral route, oral formulations are more practical for chronic treatment of patients. During clinical studies in adults, an immediate-release formulation (hard gelatine capsule) was mainly employed. A population model was recently proposed to describe MVG pharmacokinetics following both IV and oral administration in healthy adult subjects [1]. For a standard individual under fasted conditions, the bioavailability from the capsule formulation was estimated to be 44 % of the administered dose. MVG is a lipophilic neutral drug (logP of 4.7) extensively distributed to organs and tissues [2]. Its steady-state volume of distribution was estimated to be 172 l for a standard 70-kg individual and appeared to be moderately variable in a healthy adult population (coefficient of variation [CV] of 30 %) [3]. This variability was partly

Electronic supplementary material The online version of this article (doi:10.1007/s10928-015-9430-4) contains supplementary material, which is available to authorized users.

✉ Leon Aarons
leon.aarons@manchester.ac.uk

[1] Manchester Pharmacy School, The University of Manchester, Manchester, UK

[2] Drug Metabolism and Pharmacokinetics, Novartis Institutes for Biomedical Research, Basel, Switzerland

explained by body weight (BW) variations across individuals. Elimination of MVG in humans is believed to be primarily mediated by hepatic oxidative metabolism involving mainly cytochrome P450 (CYP) 3A4, 2C8, 2C9 and 2C19 [2]. Systemic clearance (CL) was reported to be moderately variable in healthy adults (32 % CV) with standard value in the population estimated to be 29.3 l/h [3].

The population pharmacokinetic model previously developed for MVG offered sufficient flexibility to describe the atypical and highly variable concentration–time data resulting from IV and oral administration in healthy adult subjects [3]. However, the empirical nature of the model allowed neither a thorough understanding of MVG pharmacokinetics nor extrapolation outside the studied population (e.g. different age or BW groups) and experimental conditions (e.g. co-administration). Conversely, physiologically-based pharmacokinetic (PBPK) models are mechanistic models that help to gain insight into the absorption, distribution and elimination behaviour of drugs. The main advantages of such models over conventional empirical models are their suitability for prediction of kinetics in various tissues and for extrapolation between species, routes of administration and dosing regimens [4]. The parameters of a PBPK model are of two types: system-specific and drug-specific. While information on system-specific or physiological parameters can be found in the literature, drug-specific parameters are typically derived from the results of pre-clinical in vitro or animal experiments. Both physiological and drug-specific parameters can carry a high degree of uncertainty. One way of introducing uncertainty during parameter estimation is to apply a Bayesian approach which yields statistical distributions of the parameter values (posterior distributions) rather than point estimates. Posterior distributions are consistent with both experimental data and prior beliefs (prior distributions of the parameters) and can be approximated by random draws using Markov Chain Monte Carlo (MCMC) simulations [5]. Also, although it has been shown that a generic whole-body PBPK (WBPBPK) model is globally structurally identifiable under certain assumptions [6], the high number of parameters and the absence of tissue data in human typically result in a numerically unstable analysis. Incorporating prior information on the parameters that are not well informed by the data can help to stabilise the analysis [7]. During drug development, it is desirable to qualify and quantify inter-individual variability (IIV) in the pharmacokinetics of tested compounds. Depending on the quality and amount of clinical data available, this can be done by performing analyses based on hierarchical models to estimate unexplained variability in the drug-specific parameters and improve individual parameter estimates [8]. A Bayesian population analysis outcomes posterior distributions not only for the individual parameters but also for the population parameters [9]. This approach has been applied successfully to physiological pharmacokinetic/toxicokinetic models [10–12] that are especially suited for separating and characterising the physiologic variability from the overall variability in the system, as clear relationships between physiological parameters and individual covariates (i.e. BW, age and gender) have been established [13, 14].

In the present study, we developed a population WBPBPK model to gain mechanistic understanding of MVG pharmacokinetics in adults. Since clinical data following IV administration in healthy adult volunteers were available, we optimised the population model using a Bayesian approach to incorporate prior pre-clinical knowledge on the drug-specific parameters. In this manner, we maintain a continuous flow of information from pre-clinical to clinical studies and possibly help stabilise the estimation of the parameters. The other aim of this study was to illustrate the ability of WBPBPK models to extrapolate pharmacokinetics across experimental conditions and studied populations. As part of MVG clinical development, the drug–drug interaction (DDI) with ketoconazole (strong CYP3A4 inhibitor) was evaluated in adults; the results (unpublished) suggested a threefold increase in the systemic exposure to MVG when orally co-administered with ketoconazole. Also, the efficacy of MVG in treating patients with fragile X syndrome was investigated. Since this mental retardation syndrome is typically diagnosed in young children [3, 15], MVG pharmacokinetics were studied in patients aged from 3 to 11 years (internal unpublished results). A powder for oral suspension (POS) was developed for drug administration in children and was assessed in adult volunteers prior to the paediatric study. Using these clinical data, we evaluated the performance of our model in predicting MVG plasma pharmacokinetics when co-administered with ketoconazole in adults or administered alone in children. To be able to predict concentration–time data after oral administration of the immediate-release formulations used in the DDI (capsule) and paediatric studies (POS), a mechanistic absorption model was also implemented. Scaling the WBPBPK model from adult to children was done by accounting for age-related anatomical/physiological changes in the studied children.

Methods

Work flow for PBPK predictions

The work flow for model development and extrapolation of MVG pharmacokinetics across formulations, dosing

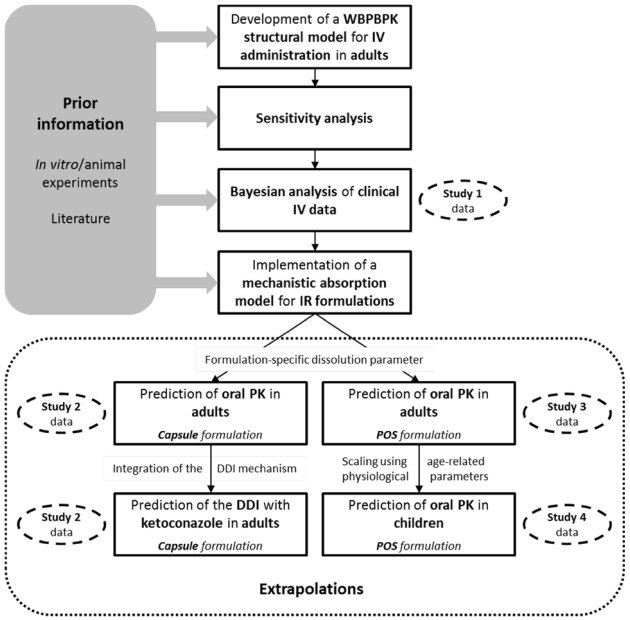

Fig. 1 Schematic work-flow of the mechanistic modelling and simulation process applied to MVG pharmacokinetics. IR denotes immediate-release. See text for definition of other symbols

regimens and age groups is depicted in Fig. 1. Firstly, a WBPBPK structural model was developed using physiological parameters from the literature and estimates of the drug-specific parameters from in vitro and animal experiments. Secondly, a sensitivity analysis of the WBPBPK model was performed to identify the drug-specific parameters that could be estimated just with plasma data. Thirdly, a hierarchical model accounting for both IIV and uncertainty in the parameters was built and optimised based on clinical IV data. Subsequently, a mechanistic absorption model for oral immediate-release formulations was implemented similarly to the disposition model. Finally, Monte Carlo simulations were performed to predict MVG pharmacokinetics under different experimental conditions (e.g. route of administration, formulation or dosing regimen) and for a different sup-population (e.g. children).

Clinical data

Plasma data from four Phase-I clinical studies (Study 1–4) were used to optimise the MVG population WBPBPK model (Study 1) and evaluate its performance in different experimental conditions and sub-populations (Study 2–4). The IV data used to optimise the disposition model (Study 1) were previously described by Wendling et al. [3]. Briefly, 120 healthy volunteers received a single 10-min IV infusion of 25 mg, 37.5 mg or 50 mg of MVG. Most subjects were young (median age of 31 years) Caucasian (62 %) male (87 %) with a median BW of 83 kg and a median body mass index of 27 kg/m^2.

Study 2 was a two-period single-sequence cross-over study conducted to quantify the impact of the co-administration of ketoconazole on MVG pharmacokinetics. During the first period, each of the 16 healthy subjects enrolled received a single 25-mg dose of MVG alone (immediate-release capsule formulation). Blood samples were collected at pre-dose, 0.5, 1, 1.5, 2, 2.5, 3, 4, 6, 12, 24, 36 and 48 h post-dose. Data from this first period were used to check the ability of the model to predict concentration–time data following oral administration of the capsule formulation in adults. Following a washout of a minimum 10 days, subjects received a repeated 400-mg daily oral dose of ketoconazole for 10 days. On Day 5 of this second period, the morning dose of ketoconazole was followed by a single oral administration of 25 mg of MVG. Only pre-dose blood samples were collected for ketoconazole. MVG blood samples were collected at pre-dose, 0.5, 1, 1.5, 2, 2.5, 3, 4, 6, 12, 24, 36, 48, 72, 96 and 120 h post-dose. Subjects were mostly young (median age of 34 years) Caucasian (88 %) male (100 %) with a median BW of 76 kg and a median body mass index of 24 kg/m^2.

Data from Study 3 were used to evaluate the ability of the mechanistic absorption model to predict plasma concentration–time profiles resulting from oral administration of the POS formulation of MVG in adults. The aim of the study was to evaluate the pharmacokinetic properties of two paediatric formulations in healthy adults, prior to studies in children. Only data for the paediatric formulation used in Study 4 were included in the present analysis. 28 healthy young (median age of 32 years) Caucasian (97 % of subjects) male received a single oral dose of 50 mg of MVG in 5 ml of suspension under fasted conditions. The studied subjects had a median BW of 82 kg and a median body mass index of 26 kg/m^2. Blood samples were collected at pre-dose, 0.25, 0.5, 1, 1.5, 2, 2.5, 3, 4, 6, 10, 14, 24, 36 and 48 h post-dose.

Study 4 was conducted to evaluate MVG pharmacokinetics after single and multiple oral administration in children with fragile X syndrome aged from 3 to 11 years [15]. Only single dose data were used to assess the ability of the WBPBPK model to extrapolate across age groups. 21 subjects received a single oral 15-mg dose of MVG POS formulation (1.5 ml of suspension after reconstitution with water). Blood samples were collected at pre-dose, 0.5, 2, 4, 8, 12 and 24 h post-dose. The demographic characteristics of the children are summarised in Table 1.

All studies were conducted according to the ethical principles of the Declaration of Helsinki and all protocols were approved by the Independent Ethics Committee or Institutional Review Board for each study center. Participants were males and non-pregnant females and all provided full written informed consent prior to inclusion in the studies. Plasma concentrations were determined by a

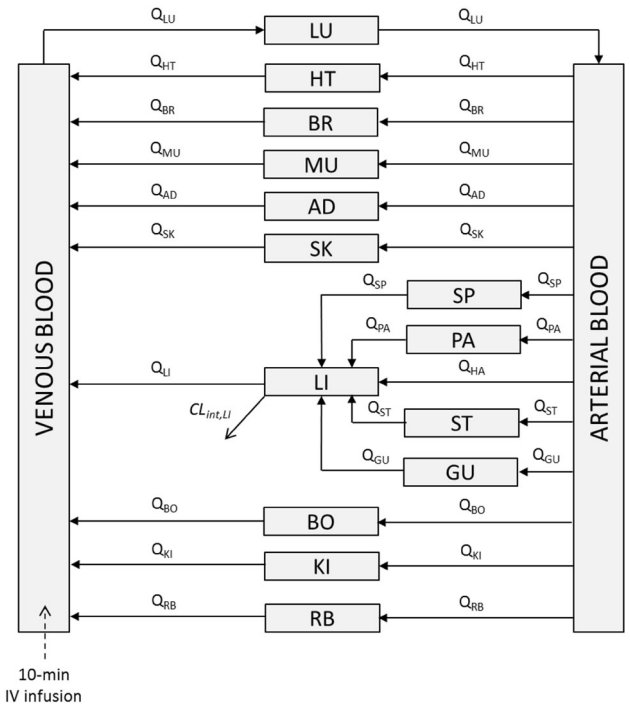

Fig. 2 Schematic representation of the WBPBPK model for MVG. See text for definition of symbols

validated liquid chromatography-tandem mass spectrometry method with a lower limit of quantification of 2 ng/ml for Study 1–3 and 0.2 ng/ml for Study 4 [16]. Concentrations below these limits were labeled as zero.

Structure of the WBPBPK model for MVG

Disposition

The WBPBPK model for MVG disposition (Fig. 2) comprises 13 tissue compartments, namely lungs (LU), heart (HT), brain (BR), muscle (MU), adipose (AD), skin (SK), spleen (SP), pancreas (PA), liver (LI), stomach (ST), gut (GU), bones (BO) and kidneys (KI). These compartments are connected together by the arterial and venous blood compartments. The LI receives blood both from the splanchnic organs (SP, PA, ST and GU) via the portal vein and directly from the hepatic artery. Since the weight of the selected tissues accounted only for 96 % of total BW, an additional rest-of-body (RB) compartment was included. All tissues were considered as well-stirred compartments, i.e. drug uptake by tissues was assumed perfusion-limited rather than permeability-limited. This assumption was deemed reasonable for a small lipophilic compound like MVG (molecular weight of 313 g/mol). The extent of drug distribution in a tissue is hence characterised by the equilibrium tissue-to-blood partition coefficient ($K_{b,T}$). The dynamics of drug amount in the tissue compartments can be described by the following equation:

$$\frac{dC_T}{dt} \cdot V_T = Q_T \left(C_{VEN/ART} - \frac{C_T}{K_{b,T}} \right) \quad (1)$$

where C_T denotes the concentration (µg/l), V_T the volume (l) and Q_T the blood flow (l/h) of the different tissues; $C_{VEN/ART}$ is either the venous (for the LU) or arterial (all other tissues) blood concentration (µg/l). The rate equations for the arterial blood (Eq. 2) and venous blood (Eq. 3) compartments were defined as follows:

$$\frac{dC_{ART}}{dt} \cdot V_{ART} = Q_{LU} \left(\frac{C_{LU}}{K_{b,LU}} - C_{ART} \right) \quad (2)$$

$$\frac{dC_{VEN}}{dt} \cdot V_{VEN} = \sum Q_T \frac{C_T}{K_{b,T}} - Q_{LU} C_{VEN} \quad (3)$$

where $\sum Q_T \frac{C_T}{K_{b,T}}$ includes all tissues except the splanchnic organs; V_{ART} is the volume of arterial blood (l) and V_{VEN} the volume of venous blood (l); Q_{LU} represents the blood flow (l/h), C_{LU} the concentration (µg/l) and $K_{b,LU}$ the partition coefficient for the LU. MVG plasma concentrations were derived by dividing C_{VEN} by the blood-to-plasma ratio BP. Based on the results of a previous pharmacokinetic study in healthy subjects [2], systemic clearance was considered to occur exclusively in the liver. The time dependency of drug amount in the liver was therefore modelled as:

$$\frac{dC_{LI}}{dt} \cdot V_{LI} = Q_{HA} C_{ART} + \sum Q_T \frac{C_T}{K_{b,T}} - Q_{LI} \frac{C_{LI}}{K_{b,LI}} - CL_{int,LI} fu_b \frac{C_{LI}}{K_{b,LI}} \quad (4)$$

Table 1 Demographic and anthropometric characteristics of Study 4 subjects

	Age (years)								
	3	4	5	6	7	8	9	10	11
Number of subjects	1	8	3	1	2	1	2	2	1
Body weight (kg)	22.4	18.8	19	23.5	20.5	28.1	33.1	51.8	45
Body surface area (m^2)	0.829	0.742	0.788	0.9	0.82	1.06	1.14	1.41	1.33

Anthropometric variables are given as median

where the sum $\sum Q_T \frac{C_T}{K_{b,T}}$ includes only the splanchnic organs; Q_{HA} is the blood flow (l/h) from the hepatic artery; C_{LI} represents the concentration (μg/l), Q_{LI} the blood flow (l/h), $K_{b,LI}$ the partition coefficient and V_{LI} the volume (l) of the liver; $CL_{int,LI}$ denotes MVG intrinsic clearance (l/h) in the liver; fu_b represents the fraction unbound in blood calculated as the ratio of the fraction unbound in plasma fu_p to BP. To describe the pharmacokinetics of MVG after IV infusion, the initial conditions of all states of the WBPBPK model were set to zero. The unit of the dose were converted from mg to μq and the unit of the infusion time from min to h in order to have an infusion rate in μq/h and concentrations in μg/l (or ng/ml). For an IV bolus of the drug, the initial condition of the venous blood compartment would be set to the administered dose.

Absorption

A three-compartment absorption model (Fig. 3) based on the compartmental absorption and transit (CAT) model was applied to the gastro-intestinal (GI) tract [17]. For simplicity, the small intestine lumen (SI) was represented by one compartment instead of seven in the CAT model. Although the simplified model doesn't describe the small intestinal transit time exactly as the CAT model, the impact on systemic absorption of MVG was deemed negligible. To account for dissolution of the dosage form, two levels distinguishing solid drug from dissolved drug were included for each segment of the GI lumen, i.e. the stomach (ST), SI and colon. The dissolution process was modelled according to Hintz and Johnson [18]. Absorption of dissolved drug was considered only in the small intestine enterocytes (ENT). Pre-systemic clearance was considered from both the ENT and LI compartments. The rate equations for each level of the ST (Eqs. 5, 6), SI (Eqs. 7, 8), colon (Eqs. 9, 10) compartments, as well as for the ENT compartment (Eq. 11) are given below:

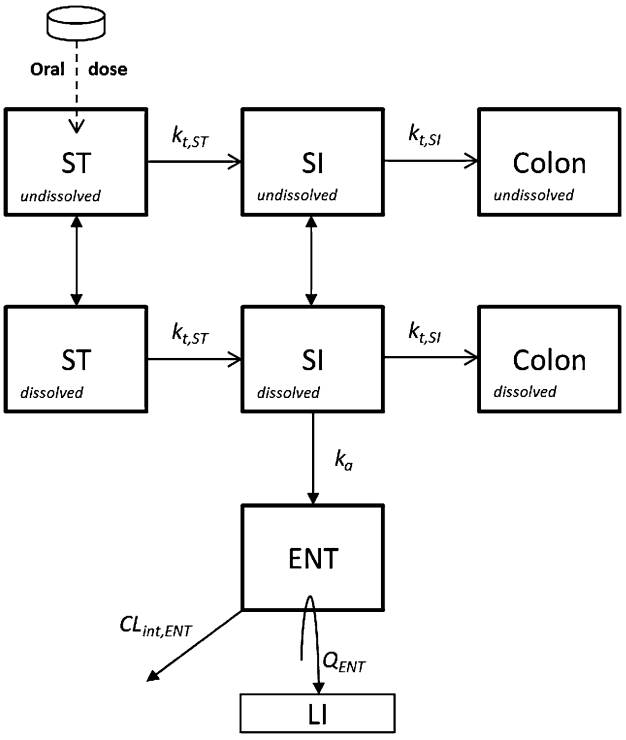

Fig. 3 Schematic representation of the mechanistic absorption model for MVG immediate-release formulations. See text for definition of symbols

$$\frac{dA_{und,ST}}{dt} = -k_{t,ST} \cdot A_{und,ST} - z \cdot \left(S_{ST} - \frac{A_{dis,ST}}{V_{ST}}\right) \cdot A_{und,ST} \tag{5}$$

$$\frac{dA_{dis,ST}}{dt} = z \cdot \left(S_{ST} - \frac{A_{dis,ST}}{V_{ST}}\right) \cdot A_{und,ST} - k_{t,ST} \cdot A_{dis,ST} \tag{6}$$

$$\frac{dA_{und,SI}}{dt} = k_{t,ST} \cdot A_{und,ST} - k_{t,SI} \cdot A_{und,SI} - z \cdot \left(S_{SI} - \frac{A_{dis,SI}}{V_{SI}}\right) \cdot A_{und,SI} \tag{7}$$

$$\frac{dA_{dis,SI}}{dt} = k_{t,ST} \cdot A_{dis,ST} + z \cdot \left(S_{SI} - \frac{A_{dis,SI}}{V_{SI}}\right) \cdot A_{und,SI} - k_{t,SI} \cdot A_{dis,SI} - k_a \cdot A_{dis,SI} \tag{8}$$

$$\frac{dA_{und,Colon}}{dt} = k_{t,SI} \cdot A_{und,SI} \tag{9}$$

$$\frac{dA_{dis,Colon}}{dt} = k_{t,SI} \cdot A_{dis,SI} \tag{10}$$

$$V_{ENT} \cdot \frac{dC_{ENT}}{dt} = k_a \cdot A_{dis,SI} - Q_{ENT} \cdot C_{ENT} - CL_{int,ENT} \cdot fu_{ENT} \cdot C_{ENT} \tag{11}$$

where $A_{und,ST/SI/Colon}$ refers to the amount (μg) of undissolved drug and $A_{diss,ST/SI/Colon}$ to the amount of dissolved drug in either the ST, SI or colon; $k_{t,ST}$ is the transit rate constant (h^{-1}) for the ST and $k_{t,SI}$ the constant for the SI; z is a dissolution constant (l/h/g) independent of the volume of medium and of drug amount and solubility [19]; S_{ST} refers to drug solubility (μg/l) in the ST and S_{SI} to that in the SI; V_{ST} refers to the volume of fluid (l) in the ST and V_{SI} to the volume in the SI; k_a is the absorption rate constant calculated as in Eq. 12; V_{ENT} represents the volume (l), C_{ENT} the concentration (μg/l), Q_{ENT} the blood flow (l/h), $CL_{int,ENT}$ the intrinsic clearance (l/h) and fu_{ENT} the fraction unbound in the ENT compartment. The effective permeability of MVG in the jejunum (P_{eff}, in cm/h) and the radii of the SI (r_{SI}, in cm) were used to estimate k_a (h^{-1}) as follows:

$$k_a = \frac{2P_{eff}}{r_{SI}} \tag{12}$$

When incorporating the absorption model into the WBPBPK model, the rate equation for the liver (Eq. 4) becomes:

$$\frac{dC_{LI}}{dt} \cdot V_{LI} = Q_{ENT}C_{ENT} + Q_{HA}C_{ART} + \sum Q_T \frac{C_T}{K_{b,T}} - Q_{LI}\frac{C_{LI}}{K_{b,LI}} - CL_{int,LI}fu_b \frac{C_{LI}}{K_{b,LI}} \tag{13}$$

All states of the full model had initial conditions equal to zero except for the state representing the undissolved drug in the stomach (Eq. 5) for which the initial condition was set to the administered dose (μq).

Statistical model

To optimise the WBPBPK model using Bayesian statistics, we developed a three-stage hierarchical model to describe both uncertainty and random IIV in the drug-specific parameters, as well as the residual difference between observations and model predictions due to model misspecification, unaccounted intra-individual variability in the parameters and measurement error. Suppose a number n_i of pharmacokinetic measurements were made for each of the K individuals, indexed by i. Denote the jth measurement for the ith individual by y_{ij} and the associated time by t_{ij}. Further, denote the p-dimensional vector of parameters for individual i by θ_i, and σ^2 the residual variance. At the first stage of the model, log-normality was assumed for the model likelihood (Eq. 14).

$$p\left(\log(y_{ij})|\theta_i, \sigma^2\right) \propto N\left(\log\left(f(D_i; t_{ij}; \theta_i)\right), \sigma^2\right), \quad i = 1, \ldots, K, \quad j = 1, \ldots, n_i \tag{14}$$

In Eq. 14, the structural model $f(\cdot)$ is a function of the ith individual-specific dosing regimen (D_i), time (t_{ij}) and parameters (θ_i). At the second stage, distributional assumptions were made for the individual-specific parameters to account for IIV (Eq. 15):

$$p(\theta_i|\mu, \Omega) = MVLN_p(\mu, \Omega), \quad i = 1, \ldots, K \tag{15}$$

where $MVLN_p(\cdot, \cdot)$ denotes a $p-$ dimensional multivariate log-normal distribution, μ is a vector of p population parameters and Ω is the $p \times p$ IIV variance–covariance matrix. At the third stage, prior distributions were assigned to both population and individual parameters to account for parameter uncertainty (Eq. 16):

$$p(\mu) = MVLN_p\left(\bar{\mu}, \sum\right), \quad p(\Omega) = IW(\Psi, \upsilon) \tag{16}$$

where $\bar{\mu}$ is a vector of p prior population parameter values; $\sum$ is the $p \times p$ variance–covariance matrix that describes the informativeness of the prior distribution of μ; Ψ is the scale matrix and υ the degree of freedom of the inverse-Wishart distribution $IW(\cdot, \cdot)$. Ψ can be calculated as $\Psi = \upsilon\bar{\Omega}$ where $\bar{\Omega}$ is the prior expectation of Ω. No prior information was considered for the variance of the residual error σ^2. The hyperparameters of the model $\bar{\mu}$, $\sum$,Ψ and υ must be stated explicitly.

A priori parameter distributions

Physiological parameters

Since WBPBPK models are mechanistic, information on system-related parameters can be extracted from the anatomy/physiology literature. To reduce the number of estimated parameters during the optimisation process and hence reduce the computational burden during the Bayesian analysis, no uncertainty in the physiological parameters was considered. The weight, density and regional blood flow for each organ/tissue of the disposition model are given in Table 2. Note that we didn't correct the organ weights for residual blood due to lack of data. However, the correction might be important for highly perfused organs like the lungs and kidneys. To account for IIV in blood flows and volumes, these parameters were related to BW of the studied subjects. More specifically, regional blood flows were expressed as fractions of the cardiac output ($f_{CO,T}$) which was in turn defined as a function of BW (Eq. 17) [20]:

$$CO_i = \left(187 \cdot BW_i^{0.81}\right) \cdot 60/1000 \qquad Q_{T,i} = f_{CO,T} \cdot CO_i \tag{17}$$

where CO_i is the cardiac output (l/h), $Q_{T,i}$ the tissue blood flow (l/h) and BW_i the BW (kg) of individual i. For each tissue of the i^{th} individual, the volume $V_{T,i}$ (l) was calculated as a fraction ($f_{BW,T}$) of BW_i corrected by the density d_T (kg/l) as in Eq. 18.

$$V_{T,i} = f_{BW,T} \cdot BW_i/d_T \tag{18}$$

To impose physiological constraints, we computed the blood flow and volume of the RB compartment by difference such that for each individual, all blood flows sum to the CO_i and all organ weights (kg) sum to the BW_i.

Drug-specific parameters

The a priori distributions of the drug-specific parameters of the WBPBPK model are summarized in the first column of Table 3. Prior distributions were constructed based on the results of an in vitro metabolism experiment and a rat distribution study performed at Novartis Pharma AG (internal unpublished data), and using in silico methods to

scale the parameters to human. The prior mean estimate of MVG hepatic intrinsic clearance $CL_{\text{int,LI}}$ (l/h) was computed by scaling the in vitro intrinsic clearances determined in recombinant human CYP enzymes. Details of the in vitro assay as well as of the extrapolation of the intrinsic clearance from the in vitro systems to human liver can be found in the Online Resource (Sect. 1). Briefly, Michaelis–Menten parameters were estimated from enzyme kinetic data for CYP 3A4, 2C8, 2C9 and 2C19. The parameter estimates were then used to calculate in vitro isoenzyme-specific intrinsic clearances which were in turn scaled to human liver as described by Howgate and co-workers [21]. The uncertainty in the Michaelis–Menten parameter estimates was propagated to the prior estimate of $CL_{\text{int,LI}}$ (26 % CV) using Fieller's theorem and other basic properties of variances (Online Resource, Sect. 1) [22].

The a priori $K_{b,T}$ estimates were computed by extrapolation of the partition coefficients determined in rat to human. Prior to clinical development, MVG pharmacokinetics was studied in rats (internal unpublished data). In short, plasma and tissue samples (LU, HT, BR, MU, AD, SK, LI and KI) were collected from 12 male rats at 0.8, 2, 8 and 24 h (3 rats per sampling time) after an IV bolus of 3 mg/kg of MVG. Concentrations were averaged at each sample time and the area under the concentration–time curve (AUC) from 0 to 24 h was calculated for each tissue using the trapezoidal method. The AUC was extrapolated to infinity by addition of the term C_{last}/λ_T where C_{last} is the plasma or tissue concentration at the last sample time and λ_T is the terminal slope of the curve. The tissue-to-plasma partition coefficients for the different tissues in rat (K_{p,T_rat}) were then calculated as follows:

$$K_{p,T\_rat} = \frac{AUC_{\text{inf},T\_rat}}{AUC_{\text{inf},plasma\_rat}} \tag{19}$$

where AUC_{inf,T_rat} is the AUC to infinity in rat tissues and $AUC_{\text{inf},plasma\_rat}$ that in rat plasma. Extrapolation of K_{p,T_rat} to human tissue-to-blood partition coefficient (K_{b,T_human}) was done with the assumption that unbound tissue-to-plasma partition coefficients are equal between rat and human (Eq. 20).

$$\begin{aligned} K_{pu,T\_human} &= K_{pu,T\_rat} = K_{p,T\_rat}/fu_{p\_rat} \\ K_{b,T\_human} &= \frac{K_{pu,T\_human} \times fu_{p\_human}}{BP} \end{aligned} \tag{20}$$

In Eq. 20 fu_{p_rat} is MVG fraction unbound in rat plasma (0.065) and fu_{p_human} that in human plasma (0.028), and K_{pu,T_rat} and K_{pu,T_human} are unbound tissue-to-plasma partition coefficients for the rat and human, respectively. Not all tissues represented in the human WBPBPK model were sampled in the rat. The equations proposed by Jansson et al. were used to predict the K_{p,T_rat} for GU and BO from the MU value [23]. However, no model was available for the K_{p,T_rat} for SP, PA and ST. Hence, K_{b,T_human} value for MU was used for these tissues as well as for the RB compartment of the WBPBPK model. Using the AUC ratio method to calculate the K_{p,T_rat} values, no estimates of uncertainty were produced. Consequently, a log-normal prior distribution with a hypothetical 30 % CV was assigned to the $K_{b,T}$ values that were estimated during the analysis of Study 1 data.

The results of the pre-clinical experiments used to calculate prior estimates of $CL_{\text{int,LI}}$ and K_{b,T_human} included no information on the variability in these parameters. However, based on our previous population pharmacokinetic analysis, MVG systemic clearance is likely to be variable in the population [3]. Perhaps just because of variability in the blood flow and volume of the liver, but the hepatic intrinsic clearance $CL_{\text{int,LI}}$ could also be variable in the population. Hence, we estimated random IIV in $CL_{\text{int,LI}}$ from the data using a diffuse inverse-Wishart distribution as prior for the variance. This was achieved by setting the degrees of freedom for the inverse-Wishart distribution equal to the dimension of the variance–covariance matrix, i.e. equal to one in our hierarchical model, as suggested in the documentation [24] of the software NONMEM 7.3.0 (ICON Development Solutions, Hanover, Maryland, USA). We assumed that population variation in the perfusion of the tissues was sufficiently accounted for by the variability in tissue volumes and regional blood flows. Also, estimating a random-effect on each of the 14 $K_{b,T}$ parameters would have considerably slowed the MCMC simulations. Therefore, the population variances of all $K_{b,T}$ values were fixed to a small value corresponding to a CV of 1 % for a log-normally distributed variable.

Sensitivity analysis of the WBPBPK model

Due to the absence of tissue data, we expected numerical instabilities to arise during optimisation of the population disposition model [7]. This is because the model's response in the venous blood compartment, and hence in plasma, is sensitive to only a few drug-specific parameters. To identify these parameters prior to model fitting, we performed a sensitivity analysis of the model. The analysis was made using 1000 sets of parameters randomly drawn from the multivariate log-normal prior distribution (CV of 26 % for the $CL_{\text{int,LI}}$ value and of 30 % for the $K_{b,T}$ values) in order to account for parameter uncertainty. For each vector of parameters, the Jacobian matrix for the venous blood compartment was calculated using the complex-step derivative approximation [25]. Further, a relative

Table 2 Physiological parameter values for the WBPBPK model

Organ/tissue	Definition	Regional blood flow[a] (%)	Weight[b] (%)	Density[c]
ART	Arterial blood	100	2.81	1.040
VEN	Venous blood	100	5.62	1.040
LU	Lungs	100	0.76	1.051
HT	Heart	4	0.47	1.030
BR	Brain	12	2	1.036
MU	Muscle	17	40	1.041
AD	Adipose	5	21.42	0.916
SK	Skin	5	3.71	1.116
SP	Spleen	3	0.26	1.054
PA	Pancreas	1	0.14	1.045
LI	Liver	25.5[d]	2.57	1.040
ST	Stomach	1	0.21	1.050
GU	Gut	14	1.44	1.043
BO	Bones	5	14.29	1.990
KI	Kidneys	19	0.44	1.050
RB	Rest-of-body	7.5	3.86	1.040

[a] Given as a percentage of the cardiac output [34]

[b] Given as a percentage of total BW [53]

[c] The value of 1.040 was used when the density was not reported [53]

[d] Total liver flow

sensitivity coefficient was calculated for each parameter of each of the 1000 sets as follows [26]:

$$RS_{VEN,pj,k} = \frac{\partial A_{VEN,j,k}}{\partial \theta_{p,k}} \cdot \frac{\theta_{p,k}}{A_{VEN,j,k}} \quad (21)$$

where $RS_{VEN,pj,k}$ is the venous blood response's relative sensitivity coefficient for the pth element of the kth vector of parameters at time j; $\frac{\partial A_{VEN,j,k}}{\partial \theta_{p,k}}$ is the $p \times j$ venous blood compartment Jacobian matrix for the kth set of parameters; $\theta_{p,k}$ is the pth element of the kth vector of parameters; $A_{VEN,j,k}$ is MVG amount in the venous blood compartment at time j, simulated with the kth set of parameters. The sensitivity of the venous blood response to the drug-specific parameters was graphically assessed across time (every 0.1 h for 48 h). For a given parameter, a relative sensitivity coefficient equal to an absolute value of 0.1 indicated that 1 % variation in the parameter value would yield 0.1 % variation in the venous blood response at a given time. Above a value of 0.1, the parameter was deemed to have a significant influence on the venous blood response and thus on the jth plasma concentration. Theoretically, only the parameters that have a significant influence on the plasma response would have their prior distributions updated by plasma data. Thus, to reduce numerical instabilities during the MCMC simulations, the drug-specific parameters deemed to have negligible impact on the plasma response were not estimated.

Bayesian computation

In the present PBPK modelling framework, a Bayesian analysis allowed prior pre-clinical beliefs on the MVG-specific parameters and information from Study 1 data to be combined. The two sources of information are complementary. During drug development, if prior knowledge at the pre-clinical stage was sufficient, clinical studies wouldn't be needed. On the other hand, due to ethical constraints, clinical data alone are insufficient to provide reasonable and precise estimates of all the parameters of such mechanistic models. Assigning prior distributions to the parameters allowed us to optimise the pharmacokinetic model while considering biological/physiological plausibility. An appealing feature of a Bayesian population approach is that the analysis yields posterior distributional estimates of the parameters of interest for the population as well as for each individual. The posterior distributions of the parameters selected based on the sensitivity analysis were approximated using random draws by Gibbs sampling as implemented in NONMEM. Observations below the lower limit of quantification were discarded from the analysis. Three independent Markov chains were initialized in parallel with different diffuse parameter values (the second and third chains were initialized with values 50 % higher and lower, respectively, than the first chain's values). A Markov chain generates samples from the target distribution only after it has converged to equilibrium. Convergence to approximate equilibrium was monitored

Table 3 Prior and posterior distributions of the drug-specific parameter values for MVG WBPBPK model

Parameter	Definition	Prior distribution	Posterior distribution	$\hat{R}$		
				n iterations ($\times 10^4$)		
				2	26	100
BP	Blood-to-plasma ratio	0.61	NE	–	–	–
fu_p	Fraction unbound in plasma	0.028	NE	–	–	–
$CL_{int,LI}$ (l/h)	Hepatic intrinsic clearance	2017 (1.30)	1606 (1.04)	1.04	1	1
K_b	Blood partition coefficient					
LU	Lungs	2.3	NE	–	–	–
HT	Heart	3.07	NE	–	–	–
BR	Brain	3.04 (1.35)	6.09 (1.16)	2.25	1.09	1.04
MU	Muscle	1.38 (1.35)	2.01 (1.07)	1.06	1.02	1
AD	Adipose	7.43 (1.35)	10.1 (1.05)	1.08	1.01	1
SK	Skin	0.592	NE	–	–	–
SP[a]	Spleen	1.38	NE	–	–	–
PA[a]	Pancreas	1.38	NE	–	–	–
LI	Liver	5.82	NE	–	–	–
ST[a]	Stomach	1.38	NE	–	–	–
GU	Gut	3.33	NE	–	–	–
BO	Bones	1 (1.35)	0.784 (1.24)	2.57	1.09	1.01
KI	Kidneys	3.73	NE	–	–	–
RB[a]	Rest-of-body	1.38 (1.35)	2.04 (1.18)	1.19	1.03	1.01
$\omega^2_{CL_{int,LI}}$	IIV in $CL_{int,LI}$	0.1 ($\upsilon = 1$)	0.161 (0.0228)	1.01	1	1
σ^2	Residual error	–	0.0815 (0.0027)	1.32	1.04	1.01

No prior information was considered for σ^2

Prior distribution was assumed multivariate log-normal for the fixed-effects and inverse-Wishart for the variance $\omega^2_{CL_{int,LI}}$

All marginal distributions are expressed as geometric mean (geometric standard deviation), except the prior of $\omega^2_{CL_{int,LI}}$ expressed as expected value (degrees of freedom), and the posterior of $\omega^2_{CL_{int,LI}}$ and σ^2 expressed as arithmetic mean (standard deviation)

NE not estimated

[a] The K_b value for the MU was used as no prior information was available

using the potential scale reduction statistic proposed by Gelman and Rubin ($\hat{R}$) [27], as well as by graphical inspection of the Markov chains. Calculation of $\hat{R}$ values was done using the software package CODA [28]. Gelman and Rubin recommend that the chains be sampled until all values for $\hat{R}$ fall below 1.10. To increase the number of samples possibly drawn from the parameter target distribution, 10^6 iterations were computed for each chain. The WBPBPK model was implemented in NONMEM as a system of 16 ordinary differential equations, which were solved during the analysis using the LSODA solver (ADVAN13 subroutine).

Monte Carlo simulations

All simulations, calculations and plots were done in MATLAB R2014a (The MathWorks, Inc., Natick, Massachusetts, USA). For each of the following prediction scenarios, Monte Carlo simulations were performed for 1000 hypothetical individuals by randomly drawing drug-specific parameters from a multivariate log-normal distribution and randomly sampling anthropometric/demographic covariates from the dataset used to evaluate the predictive performance of the model. The model predictive performance was visually assessed by computing the 5th, 50th and 95th percentiles of the simulated concentrations at each sample time, and plotting the median together with a 90 % prediction interval under the observed data.

Evaluation of the adult population disposition model

A visual predictive check of the population WBPBPK model's ability to describe Study 1 data was performed. Since Study 1 data were used to optimise the model, this step of the modelling framework can be considered as an internal validation of the population model. Plasma

concentration–time profiles were simulated by randomly sampling MVG disposition parameters from $MVLN_p(\mu, \Omega)$ and a residual error from $N(0, \sigma^2)$. μ, Ω and σ^2 were calculated by averaging the estimates from the posterior distributions, i.e. from all 10^6 iterations of the three Markov chains. For these simulations, BW was also randomly sampled from Study 1 dataset as it was a covariate for the blood flows and organ volumes.

Prediction of oral pharmacokinetics in adults

Following optimisation of the disposition model, a mechanistic absorption model was implemented to check the ability of the WBPBPK model to extrapolate from the IV route to the oral administration route. This step of the PBPK modelling framework can be seen as a pre-requisite to the prediction of the impact of DDI and age on the pharmacokinetics of orally administered MVG (Fig. 1). The structure of the model has been described earlier (Eq. 5–13) and can be applied to any oral immediate-release formulation for which in vitro dissolution data are available and can be described using the model from Hintz and Johnson (Eq. 5–8) [18]. We used the model to predict plasma concentration–time profiles following oral administration of both the capsule (Study 2) and POS formulation (Study 3) in adults. As for the WBPBPK model, the physiological parameters of the absorption model were extracted from the literature. The transit times of dosage forms in the ST and SI have been reported to be highly variable in human [17, 29, 30]. To integrate random IIV in the transit times while imposing constraints to be consistent with physiology, we assigned a logit-normal distribution to these parameters. The reported means and standard deviations (SD) were translated from the logit-normal domain (untransformed parameters) to the normal domain (logit-transformed parameters) as described by Tsamandouras and co-workers [31]. Gastric emptying and SI transit of dosage forms were assumed to be first-order processes. The transit rate constants were thus calculated as follows:

$$\begin{aligned} k_{t,ST,i} &= 1/TT_{ST,i} \\ k_{t,SI,i} &= 1/TT_{SI,i} \end{aligned} \quad (22)$$

where $k_{t,ST,i}$ is the gastric emptying rate constant (h^{-1}) and $TT_{ST,i}$ the corresponding transit time (h) for the ith individual; $k_{t,SI,i}$ is the transfer rate constant in the small intestine lumen (h^{-1}) and $TT_{SI,i}$ the small intestine transit time (h) for the ith individual. The volumes of fluid reported by Schiller et al. (means and SDs) were used to model drug dissolution in the ST and SI [32]. The mean value of 1.75 cm was used for the radius of the SI [33]. BW was randomly sampled from either Study 2 or Study 3 dataset thereby accounting for IIV in the cardiac output and organ volumes. The blood flow to the ENT represents 4.8 % of the cardiac output [34, 35]. The volume of the ENT compartment was extracted from Paine et al. and was independent of individual BW [36]. All drug-specific absorption parameters were derived from the results of in vitro experiments conducted at Novartis Pharma AG (Table 4). The formulation-specific dissolution constant z was estimated by fitting the model from Hintz and Johnson [18] to the in vitro dissolution profiles of the capsule and POS formulations (more details on the method and fitting results in Sect. 2 of the Online Resource). P_{eff} was derived from the apparent permeability coefficient determined in an in-house Caco-2 cell monolayer system, and using the in silico method described by Sun et al. to scale from the in vitro system to human jejunum [37] (details in Sect. 3 of the Online Resource). For each of the 1000 hypothetical individual, MVG enterocytic intrinsic clearance $CL_{\text{int,ENT}}$ (Eq. 11) was computed by first back-calculating the recombinant human CYP-specific intrinsic clearances (see Eq. 2 in Sect. 1 of the Online Resource) from $CL_{\text{int,LI}}$, then scaling from the recombinant systems to small intestine enterocytes as described by Howgate et al. [21]. The assumed contributions of CYP3A4 (73 %), CYP2C8 (5 %), CYP2C9 (17 %) and CYP2C19 (5 %) to MVG hepatic metabolism were calculated using our prior in vitro estimates of the CYP-specific intrinsic clearances in human liver microsomes (see Eq. 2 in Sect. 1 of the Online Resource). We assumed that only CYP3A4, CYP2C9 and CYP2C19 enzymes contributed to MVG gut wall metabolism. The abundance of these enzymes in the ENT was extracted from Sjogren et al. [38]. When no information on variability in the absorption parameters was available, a CV of 30 % was included in the present Monte Carlo simulations. The performance of the full model (absorption and disposition) in predicting MVG pharmacokinetics following oral administration of both the capsule and POS formulation was visually assessed as described earlier, using data from Study 2 and Study 3. To gain insight into the effect of first pass metabolism on MVG systemic exposure, the simulations were used to calculate the fraction of dose absorbed into the gut wall (F_a), the fraction escaping gut wall metabolism (F_g) and the fraction escaping hepatic extraction (F_h) for both the capsule and POS formulation (details in Sect. 4 of the Online Resource).

Prediction of the DDI with ketoconazole in adults

To check the ability of the population PBPK model to extrapolate across dosing regimen, we used the full model to predict MVG pharmacokinetics following oral co-administration with ketoconazole in adults (Study 2). As described in Fig. 1, these simulations were conditional on

the success of MVG pharmacokinetic predictions for the capsule formulation (first period of Study 2). Ketoconazole is a strong competitive inhibitor of CYP3A4 [39] and a moderate one of CYP2C8 [40] and CYP2C9 [41]. In the presence of a competitive inhibitor, the intrinsic clearance of a CYP substrate can be expressed as follows:

$$CL'_{int,CYP_i} = \frac{CL_{int,CYP_i}}{\left(1 + \frac{[I]_u}{K_{i,u,CYP_i}}\right)} \quad (23)$$

where CL'_{int,CYP_i} is the isoenzyme-specific intrinsic clearance (l/h) in the presence of inhibitor and CL_{int,CYP_i} the clearance in the absence of inhibitor; $[I]_u$ is the inhibitor unbound concentration (μM) in the tissue of interest; K_{i,u,CYP_i} is the isoenzyme-specific unbound inhibition constant (μM). CL_{int,CYP_i} values were derived from $CL_{\text{int,LI}}$ values using our prior belief of the CYP enzymes' contribution to MVG hepatic metabolism described earlier. $[I]_u$ was calculated as the product of the inhibitor tissue concentration by the fraction unbound in the tissue. K_{i,u,CYP_i} was defined as the product of the isoenzyme-specific inhibition constant and the unbound fraction of inhibitor in microsomes. Tissue concentrations of ketoconazole were simulated with Simcyp Version 13 (Simcyp Limited, Sheffield, UK) and the design of Study 2 (400-mg/day for 10 days). Using the minimal PBPK model implemented in Simcyp [42], it is possible to simulate ketoconazole total concentrations in the portal vein and liver (see Fig. 2 in Sect. 5 of the Online Resource). To derive ketoconazole unbound concentrations in the liver, the fraction unbound in the liver was calculated as the ratio of the fraction unbound in plasma to the liver-to-plasma partition coefficient for ketoconazole. To compute ketoconazole unbound concentrations in the ENT, we assumed that total concentrations in the portal vein reflect those in the ENT [42], and used ketoconazole fraction unbound in the ENT to derive unbound concentrations. We resorted to Simcyp default values of the inhibition-related ketoconazole parameters for the present simulation (Table 2 in Sect. 5 of the Online Resource). The simulated ketoconazole concentration–time data were used as forcing functions for the inhibition of the intrinsic clearance in the ENT and LI compartments (Eq. 4, 11 and 23). Interpolation of ketoconazole concentrations from the Simcyp-produced sample times to each time step used by the differential equation solver in MATLAB was done using the function 'interp1' (spline interpolation method). To account for uncertainty in the ketoconazole inhibition constant values reported by Simcyp, simulation of MVG concentration–time profiles was performed assuming a CV of 30 % for these parameters. Data from the second period of Study 2 were used to visually evaluate the performance of the model in predicting the impact of the MVG-ketoconazole interaction on MVG pharmacokinetics. To check the consistency of the PBPK modelling approach with the standard non-compartmental analysis approach used to quantify the impact of DDIs on drug pharmacokinetics, we calculated for each hypothetical individual the change in AUC to infinity when MVG was co-administered with ketoconazole compared to when administered alone.

Prediction of oral pharmacokinetics in children

The suitability of the WBPKPK model for extrapolation of MVG pharmacokinetics from adults to paediatrics was evaluated using data from Study 4. As schematically explained in Fig. 1, this simulation was conditional on the ability of the model to predict pharmacokinetics of the POS formulation in adults (Study 3). Children enrolled in Study 4 were diagnosed with Fragile X syndrome. We assumed that the disease had no impact on MVG pharmacokinetics. Hence, the model was scaled from adult to children by simply integrating the age-related physiological changes in children from 3 to 11 years of age. Information on the age dependencies of the physiological parameters was gathered from the literature for age groups of 1, 5, 10 and 15 years. As for the adult WBPBPK model, regional blood flows were expressed as fractions of the cardiac output, $f_{CO,T}$, (Eq. 17) and organ volumes as fractions of BW, $f_{BW,T}$, (Eq. 18), thereby accounting for variability in tissue perfusion. The cardiac output was defined as a function of both children's age and body surface area (BSA) as described by Johnson et al. [43]. $f_{CO,T}$ values were computed using the reported age-specific values of the cardiac output [34] and regional blood flows [44]. $f_{BW,T}$ values were calculated based on age-related changes in BW and actual organ weights [34]. The same densities as for adults were used for most organs/tissues except for the bones for which information was available in the literature [34]. For this simulation, age and BSA were randomly sampled from Study 4 dataset for each of the 1000 hypothetical individuals. The MATLAB 'interp1′ function (spline interpolation method) was used to interpolate the physiological parameters from the reference age groups to each individual age. MVG fraction unbound in plasma fu_p was also scaled from adult to children as described by Johnson et al. [43]. For each of the 1000 hypothetical children, the hepatic intrinsic clearance was derived by simply back-calculating the total intrinsic clearance in human liver microsomes from the adult $CL_{int,LI}$ (see Eq. 2 in Sect. 1 of the Online Resource), then scaling it again to human liver using the liver weight of the hypothetical child. We thereby assumed that the IIV in $CL_{int,LI}$ (estimated from Study 1 data) is the same between adults and children as we had no prior information on the variability in $CL_{int,LI}$ in children. Based on the ontogeny of CYP enzymes [45], we assumed that all

Table 4 Drug-specific parameters of the absorption model for MVG oral immediate-release formulations

Parameter	Definition	Estimate	Source
$z_{capsule}$ (10^{-4} l/h/g)	Dissolution constant for the capsule	0.124	Fit to in vitro dissolution profile
z_{POS} (10^{-4} l/h/g)	Dissolution constant for the POS	2.04	Fit to in vitro dissolution profile
S_{ST} (10^{6} ng/ml)	Drug solubility in stomach	0.019	In vitro solubility experiment[a]
S_{SI} (10^{6} ng/ml)	Drug solubility in small intestine	0.037	In vitro solubility experiment[b]
P_{eff} (cm/h)	Jejunal effective permeability	5.1	In vitro Caco-2 experiment together with in silico model from Sun et al. [37]
fu_{ENT}	Fraction unbound in enterocytes	fu_p	Assumption based on Yang et al. [54]

[a] Determined in fasted state simulated gastric fluid

[b] Determined in fasted state simulated intestinal fluid

enzymes involved in MVG metabolism achieved complete maturity in children aged from 3 to 11 years (same abundances in the ENT and LI as in adults). Finally, to account for variation in drug dissolution between adults and children, the volume of fluid in the SI, V_{SI} (Eq. 7, 8) was defined as a fraction of the volume of the SI cylinder which was calculated using BSA-dependent diameter and length of the SI [43]. The fraction of the cylinder was derived using the adult volume of fluid V_{SI} [32] and volume of the SI cylinder [46] values. The predictive performance of the model for children was graphically evaluated as for the other simulation scenarios.

Results

Figure 4 shows the results of the sensitivity analysis of the WBPBPK model (disposition only). For each parameter of each of the 1000 parameter vectors drawn from the prior distribution, the absolute value of the venous blood relative sensitivity coefficient $RS_{VEN,pj,k}$ (Eq. 21) was plotted across time. These results suggest that $CL_{int,LI}$, $K_{b,MU}$ and $K_{b,AD}$ are the parameters that have the main influence on the venous blood response, but that the response might be also slightly sensitive to the $K_{b,BR}$, $K_{b,BO}$ and $K_{b,RB}$ parameters. Therefore, only six drug-specific parameters out of 15, namely $CL_{int,LI}$, $K_{b,MU}$, $K_{b,AD}$, $K_{b,BR}$, $K_{b,BO}$ and $K_{b,RB}$, were estimated during the Bayesian analysis of Study 1 data.

The posterior distribution of these parameters as well as of the population variance of $CL_{int,LI}$ ($\omega^2_{CL_{\text{int,LI}}}$) and of the residual variance (σ^2), are summarized in Table 3 and were obtained by pooling the one million parameter vectors from all three Markov chains. On average, one million iterations were completed in approximately 11 days on a medium-sized cluster running Red Hat Enterprise Linux 6.5 on nodes with Intel Xeon E5-2670v2 CPUs with some older nodes running with dual Xeon X5670 CPUs. Each chain was parallelized on 12 different nodes. The nodes are equipped with between 24 and 96 GB of RAM and are interconnected vial dedicated Bonded 1 Gbit network cards. As indicated by the $\hat{R}$ statistic (Table 3), convergence to the target distribution was achieved after 20,000 iterations for $CL_{int,LI}$, $K_{b,MU}$, $K_{b,AD}$ and $\omega^2_{CL_{\text{int,LI}}}$ but not for $K_{b,BR}$, $K_{b,BO}$, $K_{b,RB}$ and σ^2. The distribution of the latter seemed to eventually reach equilibrium after 260,000 iterations. Trace-plots of the three Markov chains run to approximate the posterior distribution are presented in Fig. 5 and show a slower mixing of the chains for the parameters $K_{b,BR}$, $K_{b,BO}$ and $K_{b,RB}$ than for the other parameters. A comparison of the marginal prior and posterior distribution of the parameters for which we had prior knowledge is presented in Fig. 6. All estimated parameter distributions were updated by Study 1 plasma concentration–time data, and appeared to be normal and within plausible biological/physiological limits. The smallest change from the prior mean estimate was for the population estimate of $CL_{int,LI}$ (1.26-fold decrease). The most notable deviation was observed for the estimate of $K_{b,BR}$ that doubled from the value of 3.04. Overall, the uncertainty in all population parameter values was reduced, especially for $CL_{int,LI}$, $K_{b,MU}$ and $K_{b,AD}$ for which the uncertainty CV decreased to a value of 4, 7 and 5 %, respectively. As suggested by the small uncertainty in $\omega^2_{CL_{\text{int,LI}}}$ (CV of 14 %), variability in $CL_{int,LI}$ was well informed by the data and appeared to be high in the studied healthy adult subjects (CV of approximately 108 %). The residual error, which accounts for unexplained intra-individual variability, model misspecification and analytical error for observations in plasma, had a small variance estimate (Table 3) thereby indicating a good fit of the model to Study 1 data.

Figure 7 shows a visual predictive check of the population model's ability to describe Study 1 data. Observed and simulated concentrations were dose-normalised. Both the median trend and the variability in the data seem to be well captured by the model, confirming the suitability of the population WBPBPK model to describe MVG disposition in adults.

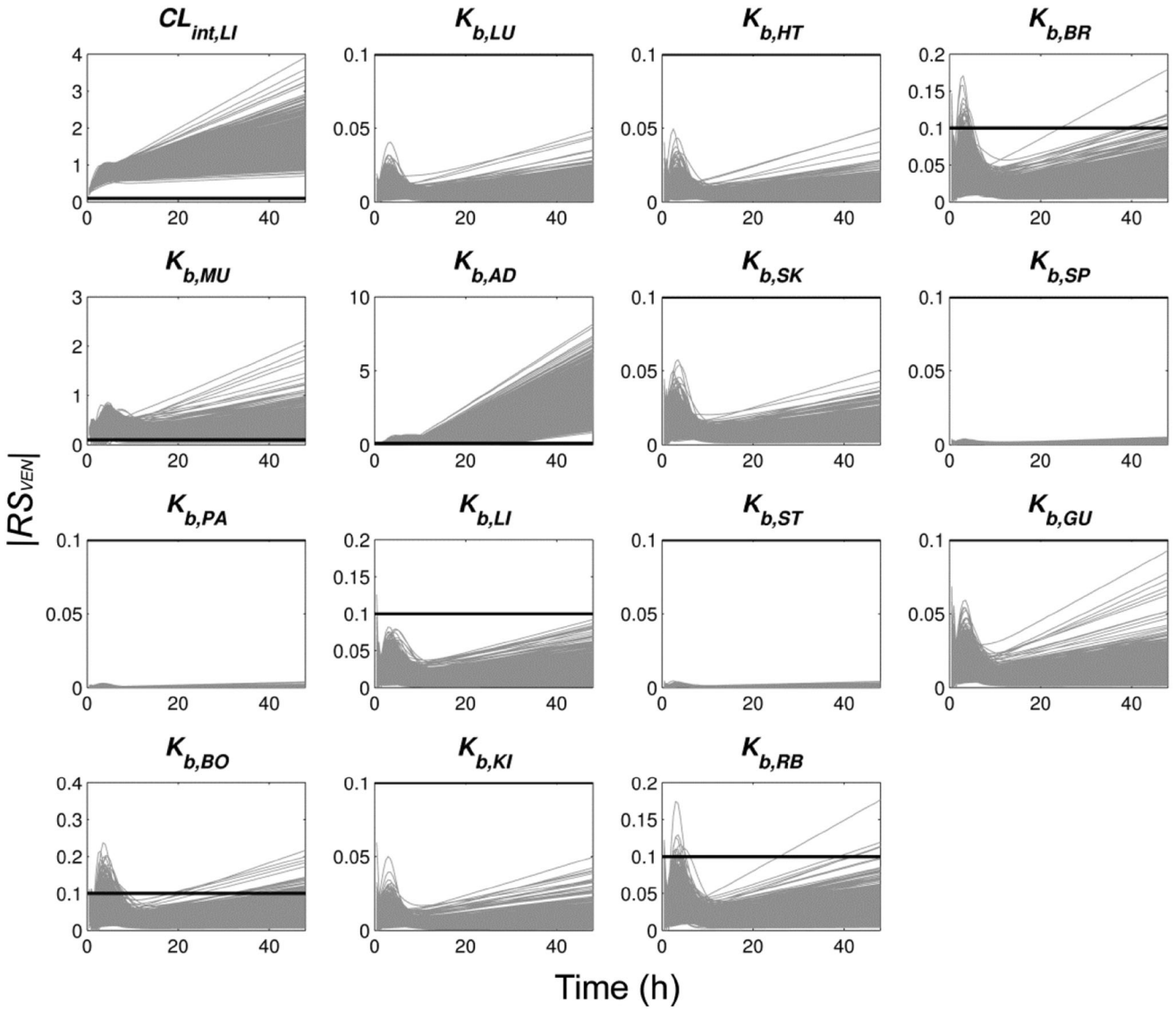

Fig. 4 Absolute value of the relative sensitivity coefficient for the venous blood compartment $|RS_{VEN}|$ (*solid grey lines*) plotted against time for each parameter of each of the 1000 parameter vectors drawn from the prior distribution. The *horizontal solid black line* represents the threshold value of 0.1 used to assess the influence of a parameter on the venous blood response: a coefficient higher than this value suggests a significant influence on the response. See text for definition of symbols

The results of the Monte Carlo simulations for extrapolation of MVG pharmacokinetics beyond Study 1 population and experimental conditions are presented in Fig. 8. For each simulation scenario, the model could predict reasonably well both the median trend and the variability in MVG plasma concentration–time data, which shows the adequacy of the population PBPK model for extrapolation across routes of administration and formulations (Fig. 8a, b), dosing regimen (Fig. 8c) and age groups (Fig. 8d). Nevertheless, the variability in the early concentration–time data is overall slightly under-predicted (see Fig. 8b, c). Moreover, the model slightly over-predicts the median trend in the paediatric data, especially during the first 5 h post-dose during which drug absorption occurs. In adults, the geometric mean value of the simulated F_a was slightly higher for the POS formulation (0.65) than for the capsule formulation (0.52). However, taking into account the variability, there was no statistically significant difference between the F_a values of the two formulations (the 90 % confidence interval was [0.34; 0.73] for the capsule and [0.39; 0.87] for the POS formulation). The geometric mean values of F_g and F_h were 0.93 (CV of 3 %) and 0.64 (CV of 17 %), respectively, regardless of the formulations. The DDI simulations suggest that on average, the systemic

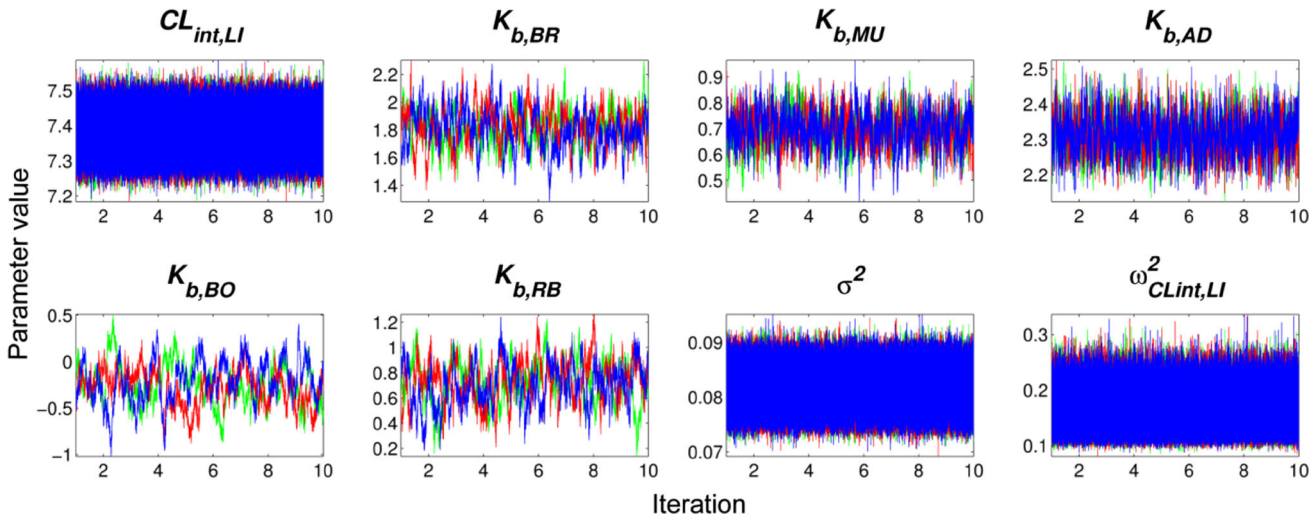

Fig. 5 Trace-plots of the three Markov chains run for the Bayesian population analysis of Study 1 data. Log-transformed parameter values (except for σ^2 and $\omega^2_{CL_{int,LI}}$) are plotted against the number of iteration ($\times 10^5$) of the MCMC simulations. See text for definition of symbols (Color figure online)

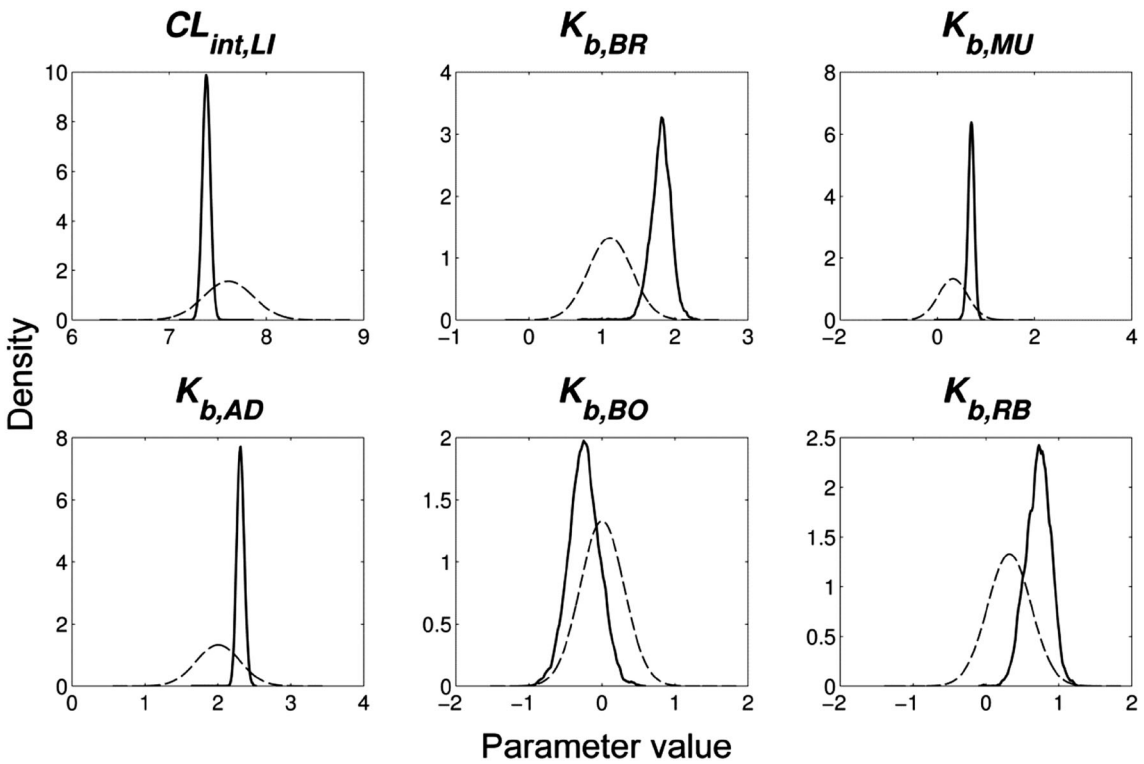

Fig. 6 Posterior (*solid lines*) and prior (*dashed lines*) marginal densities of the log-transformed population parameters of MVG WBPBPK model estimated during the Bayesian population analysis of Study 1 data. See text for definition of symbols

exposure to MVG is increased by 3.8 fold (geometric mean of the AUC ratio) when co-administered with 400 mg of ketoconazole compared to administration of MVG alone. However, this increase in systemic exposure might be highly variable in a healthy adult population (90 % confidence interval of [1.4; 9.8]).

Discussion

We have reported the development, optimisation and applications of a population WBPBPK model for MVG to gain understanding of its pharmacokinetics during its clinical development and to evaluate the ability of the model to

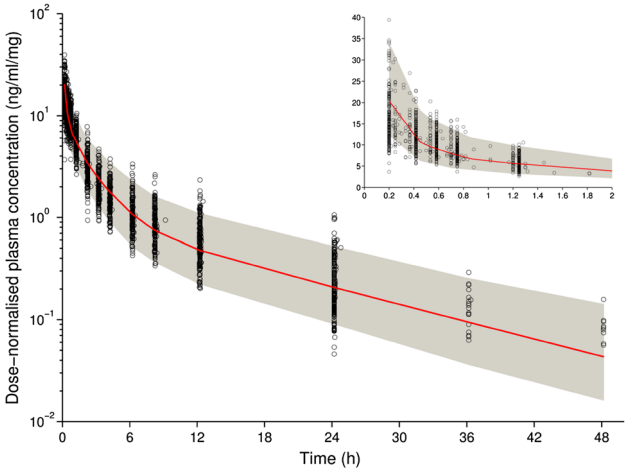

Fig. 7 A visual predictive check of the population WBPBPK model's ability to describe Study 1 data. *Open circles* are observed concentrations plotted across time, the *solid red line* is the median of the simulated concentrations and the *grey area* represents a 90 % prediction interval. Both observed and predicted concentrations were dose-normalised. The insert expands the first 2 h of the concentration–time data plotted on linear scales (Color figure online)

extrapolate beyond the data analysed. Since the generic WBPBPK model proposed is mechanistic in nature, its parameters could be defined a priori using knowledge from the literature (system-specific parameters) and pre-clinical experiments (drug-specific parameters). Bayesian statistics were applied to leverage our prior knowledge of the drug-specific parameters while avoiding biologically unrealistic estimates as well as numerical instabilities due to the absence of tissue data. Using a Bayesian population approach, the current pharmacokinetic model could be progressively updated by new clinical data in order to propagate the information throughout the drug development process.

To decrease the computational burden during the MCMC simulations, we estimated only the parameters that were deemed to have a significant influence on the venous blood response. Although this approach can be considered subjective, we believed that accounting for uncertainty in all parameters of the WBPBPK model, including physiological parameters (i.e. blood flows and organ volumes), would have yielded significant numerical instabilities given

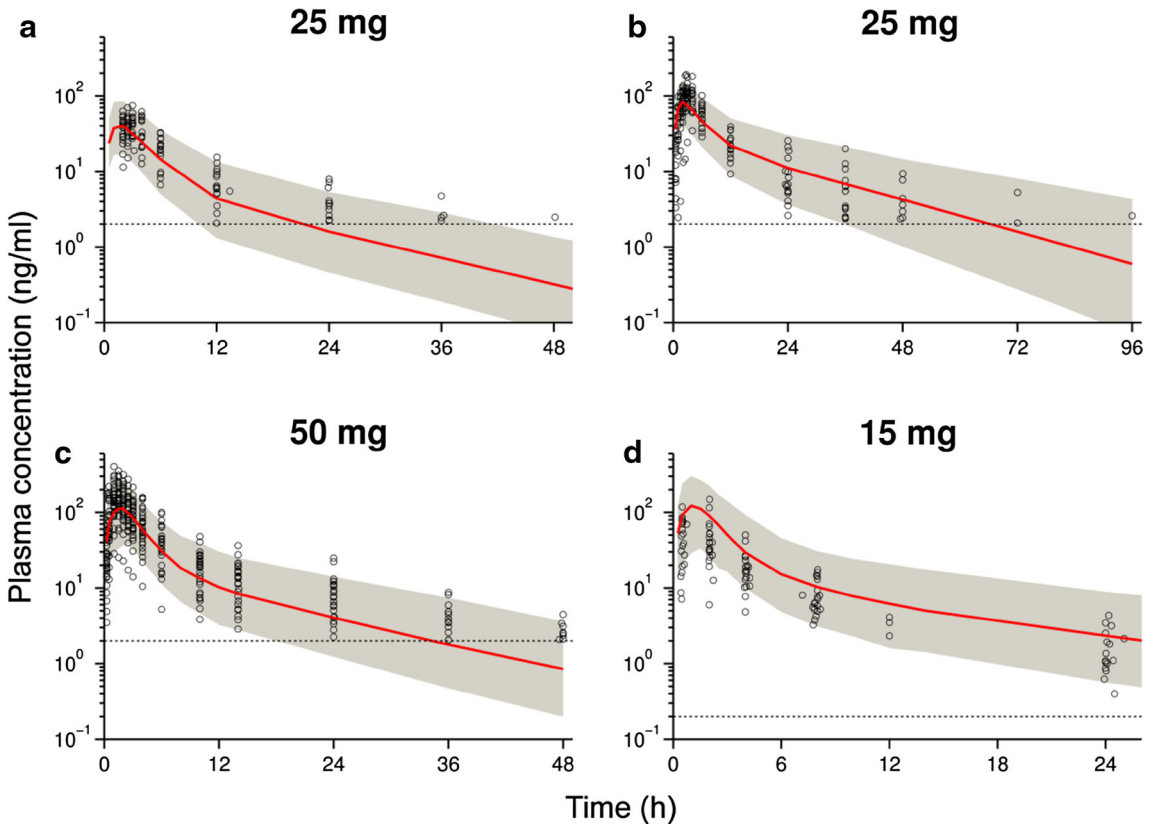

Fig. 8 A visual evaluation of the model's ability to predict MVG pharmacokinetics when orally administered alone in adults using either the capsule (**a**) or the POS formulation (**c**), when co-administered with ketoconazole in adults using the capsule formulation (**b**), and when administered alone in children using the POS formulation (**d**). *Open circles* are observed concentrations plotted across time, the *solid red lines* are the medians of the simulated concentrations and the *grey areas* represent 90 % prediction intervals. The *horizontal dotted black lines* represent the lower limit of quantification of the assays (Color figure online)

the available data. In fact, a preliminary analysis of Study 1 data in which we estimated all drug-specific parameters (but not the physiological parameters) showed that the posterior distribution of the parameters couldn't reach approximate equilibrium even after one million iterations (Fig. 3 in Sect. 6 of the Online Resource) possibly because of high correlations between parameters and/or because the priors were too vague given the complexity of the model. Hence, we decided to estimate only the six drug-specific parameters selected based on the results of the sensitivity analysis. An alternative to this approach could be to reduce the WBPBPK model using proper lumping techniques [47] to possibly shorten the data analysis and stabilise the MCMC simulations. Using proper lumping, the parameters of the lumped compartments can be directly related to the parameters of the original model. Hence, prior knowledge on the parameters of the WBPBPK model can be used to construct prior distribution of the reduced model parameters. Nevertheless, an optimal lumping scheme for a model is specific to its structure and distribution of the parameter values. Therefore, the use of reduced PBPK models for extrapolation of pharmacokinetics across experimental conditions and sub-populations is challenging as it often requires the incorporation of additional mechanisms in the model (e.g. DDI mechanism) and/or to scale the parameter distributions (e.g. from adult to children).

The Bayesian population analysis of Study 1 data provided better and more precise estimates of the population parameters $CL_{int,LI}$, $K_{b,MU}$, $K_{b,AD}$,$K_{b,BR}$, $K_{b,BO}$ and $K_{b,RB}$ while maintaining biologically plausible values (Table 3). The data contained information mostly for $CL_{int,LI}$, $K_{b,MU}$ and $K_{b,AD}$ as indicated by the higher reduction in the uncertainty in these parameters compared to the other parameters (Fig. 6). This is consistent with the results of the sensitivity analysis (Fig. 4) and with the fact that target distributions were reached much faster for $CL_{int,LI}$, $K_{b,MU}$ and $K_{b,AD}$ (20,000 iterations) than for $K_{b,BR}$, $K_{b,BO}$ and $K_{b,RB}$ (260,000 iterations) during the MCMC simulations. The estimates of the tissue-to-blood partition coefficients indicate that MVG is extensively distributed into the adipose tissue and the brain (target site), which was expected for a small neutral lipophilic drug that is a priori not substrate to any efflux transporter [2]. Our simulations suggest that on average, the brain exposure might be four times higher than the plasma exposure to the drug. Although we have no data to check whether these predictions are reasonable or not, exploratory simulations can be performed to evaluate the impact of the brain exposure on drug response under different scenarios as well as the sensitivity of the system to parameter uncertainty and variability. Such exposure–response simulation study can be of clinical value to predict a dosing regimen that best fits efficacy or safety requirements.

Using a population approach, we could quantify IIV in $CL_{int,LI}$, even though we didn't have prior knowledge of the variability in this parameter. This variability is likely explained by the heterogeneity of the CYP enzymes' functionality within the human population. For instance there is evidence for genetic polymorphism of CYP2C9 [48]. Information on individual genotypes was however not available and could therefore not be tested in the population model as a covariate for $CL_{int,LI}$. Note that the high variance estimate for $CL_{int,LI}$ could be inflated if variability in the physiological parameters was underestimated. In this study, we chose BW as explanatory variable for the physiologic variability in the organ volumes and blood flows. However, there is evidence that for a given age and gender, the variability in the organ volumes is better correlated with body height (e.g. heart, lungs and liver) or independent of BW and body height (e.g. brain), and that the variability in the blood flows is better explained by body height [14]. This should be taken into consideration if the model were to be used for exploratory simulations, especially for prediction of the target site exposure to the drug as discussed in the previous paragraph.

Before discussing the results of our Monte Carlo simulations, it should be stressed that the simulations were performed without taking into account the uncertainty around the population and individual parameter estimates, meaning that our predictions represent the mean of the predictions derived using the full posterior parameter density. Making full use of the posterior parameter distribution can be of value during drug development to account for parameter uncertainty when predicting clinical endpoints. However, the objective of the present simulations was to evaluate the ability of the model to extrapolate MVG pharmacokinetics rather than to address specific efficacy or safety concerns.

Incorporating a mechanistic absorption model into the WBPBPK model allowed extrapolation of MVG pharmacokinetics from the IV administration route to the oral route. The prior knowledge that we had on the system-, drug- and formulation-specific parameters appeared good enough for prediction of MVG oral pharmacokinetics without having to optimise any absorption parameters (Fig. 8a, b), although the slight under-prediction of the variability at the early time points suggests that the absorption parameters might be more variable than what we accounted for. An advantage of this so-called "bottom-up" approach is that, using available formulation-specific dissolution data, the model can be applied to predict pharmacokinetics of other oral immediate-release

formulations of interest. This can be of value during clinical development to anticipate the dose that would yield a desirable steady-state exposure for a new formulation. In our work, this was rather a pre-requisite to be able to predict the impact of the DDI with ketoconazole on the pharmacokinetics of the capsule formulation in adults, and predict the pharmacokinetics of the POS formulation in children. Of note, more complex models could be implemented to describe more mechanistically the dissolution process [19, 49, 50]. Another advantage of mechanistic absorption models is that a better understanding of the systemic bioavailability and the first-pass effect can be gained. Our simulations suggest that for both the capsule and POS formulation, on average more than 50 % of an orally administered dose of MVG is absorbed into the gut wall. This is consistent with the reported results of a clinical study of the pharmacokinetics of ^{14}C-radiolabeled MVG orally administered to four healthy adult subjects using the capsule formulation [2]. The high value of F_g (0.93) indicates a low extent of gut wall metabolism of MVG, which however strongly relies on our assumption that the drug is bound to proteins in the enterocytes to the same extent as in the plasma. The systemic bioavailability of MVG was predicted for a standard individual in the population to be 31 % for the capsule and 39 % for the POS formulation. It should be noted that the capsule formulation used in Study 2 is different from the capsule formulation assessed in our previous population analysis of MVG pharmacokinetics in healthy adults (different dissolution characteristics) [3]. Therefore, it wasn't relevant to compare the present estimate of the systemic bioavailability with the one from our previous analysis.

One of the main applications of PBPK models is to predict the impact of DDIs on pharmacokinetics of therapeutic drugs. Since our population WPBPK model could adequately predict the pharmacokinetics of the capsule formulation in the adult subjects of Study 2, we subsequently used it to predict the effect of ketoconazole on MVG pharmacokinetics, without using the data to optimise the inhibition-related parameters. The model predictions were in good agreement with the available clinical data (Fig. 8c). In addition, the predicted increase in AUC (3.8-fold) was consistent with the results (unpublished) of a former in-house non-compartmental analysis of Study 2 data (three-fold). Nevertheless, other types of DDIs (e.g. mechanism-based inhibition and induction) should be investigated with the proposed PBPK model to gain confidence in the metabolic pathways involved in MVG elimination. Moreover, since MVG can be associated to serious neurological adverse events [51, 52] and since its efficacy is believed to be closely related to the brain exposure, it is important to identify DDIs that have significant effect on brain concentrations in order to suggest possible dose adjustments.

It has been recognised that the PBPK modelling approach is ideal for extrapolation of pharmacokinetics of therapeutic drugs from an adult to a paediatric population because the differences in the concentration–time profiles are mainly due to age-related differences in anatomy and physiology [44]. Including the age-related changes in the physiological parameters of our WPBPK model as well as in some drug-specific parameters (i.e. fu_p and $CL_{in,LI}$) allowed reasonable prediction of MVG pharmacokinetics in children from 3 to 11 years of age, without having to fit the model to the clinical data (Fig. 8d). The over-prediction of the median pharmacokinetic trend in the first 5 h post-dose could be explained by unaccounted age-related changes in the absorption parameters. No strong evidence of differences in the absorption-related physiological parameters (e.g. gastric and small intestine transit times) between adults and children could be found in the literature. However it is likely that dissolution of the POS formulation (rate-limiting step of MVG absorption) has a different pattern in children compared to adults possibly because the dynamic of fluid in the small intestine is different and/or the change in the fluid volume is more important than what we accounted for. Nevertheless, the 21 children enrolled in Study 4 might not be representative of a population aged from 3 to 11 years (see Table 1) which could also explain the discrepancies between the model predictions and the observations. It should also be noted that the maturation of CYP enzymes involved in MVG metabolism was considered to be achieved in children aged from 3 years. To predict pharmacokinetics in younger subjects, age-related changes in the enzyme abundances (both in the liver and gut wall) should be incorporated in the model using ontogeny equations [45].

Conclusions

In conclusion, population physiological modelling of MVG pharmacokinetics provided further insight into its absorption, distribution and elimination mechanisms in human, including the source and magnitude of variability. The Bayesian approach offered a continuous flow of information from pre-clinical to clinical studies and helped to reduce the uncertainty in some drug-specific parameter values. This approach could be applied to new clinical data to update our current knowledge of MVG population pharmacokinetics and maintain the information flow during drug development. The model can be used to predict plasma and brain (target site) concentration–time profiles following administration of various oral immediate-release formulations of MVG alone or when co-administered with other drugs, in adults as well as in children. While predicting the pharmacokinetic

properties of new formulations is not of particular interest for the current clinical development of MVG, being able to predict the DDI risk of compounds likely to be co-administered with MVG, across different age groups, could be useful for the design of better clinical studies. For that purpose, the data used to evaluate the predictive performance of the model (Study 2–4) could now be analysed to improve our current estimates of the parameters.

Acknowledgments The authors would like to thank Nikolaos Tsamandouras and Andres Olivares-Morales (Manchester Pharmacy School, The University of Manchester, Manchester, United-Kingdom) for fruitful discussions.

Compliance with ethical standards

Conflict of interest Thierry Wending is an employee of Novartis Pharma AG and a Ph.D. student at the University of Manchester.

References

1. Wendling T, Ogungbenro K, Pigeolet E, Dumitras S, Woessner R, Aarons L (2015) Model-based evaluation of the impact of formulation and food intake on the complex oral absorption of mavoglurant in healthy subjects. Pharm Res 32(5):1764–1778. doi:10.1007/s11095-014-1574-1
2. Walles M, Wolf T, Jin Y, Ritzau M, Leuthold LA, Krauser J, Gschwind HP, Carcache D, Kittelmann M, Ocwieja M, Ufer M, Woessner R, Chakraborty A, Swart P (2013) Metabolism and disposition of the metabotropic glutamate receptor 5 antagonist (mGluR5) mavoglurant (AFQ056) in healthy subjects. Drug Metab Dispos 41(9):1626–1641. doi:10.1124/dmd.112.050716
3. Wendling T, Ogungbenro K, Pigeolet E, Dumitras S, Woessner R, Aarons L (2014) Model-based evaluation of the impact of formulation and food intake on the complex oral absorption of mavoglurant in healthy subjects. Pharm Res. doi:10.1007/s11095-014-1574-1
4. Edginton AN, Theil FP, Schmitt W, Willmann S (2008) Whole body physiologically-based pharmacokinetic models: their use in clinical drug development. Expert Opin Drug Metab Toxicol 4(9):1143–1152. doi:10.1517/17425255.4.9.1143
5. Wakefield JC, Smith AFM (1994) Bayesian analysis of linear and non-linear population models by using the Gibbs sampler. Appl Stat 43:201–221
6. Yates JW (2006) Structural identifiability of physiologically based pharmacokinetic models. J Pharmacokinet Pharmacodyn 33(4):421–439. doi:10.1007/s10928-006-9011-7
7. Tsamandouras N, Rostami-Hodjegan A, Aarons L (2015) Combining the 'bottom up' and 'top down' approaches in pharmacokinetic modelling: fitting PBPK models to observed clinical data. Br J Clin Pharmacol 79(1):48–55. doi:10.1111/bcp.12234
8. Sheiner LB (1984) The population approach to pharmacokinetic data analysis: rationale and standard data analysis methods. Drug Metab Rev 15(1–2):153–171. doi:10.3109/03602538409015063
9. Wakefield JC (1996) The Bayesian analysis of population pharmacokinetic models. J Am Stat Assoc 91:61–76
10. Bois FY, Gelman A, Jiang J, Maszle DR, Zeise L, Alexeef G (1996) Population toxicokinetics of tetrachloroethylene. Arch Toxicol 70(6):347–355
11. Jonsson F, Johanson G (2001) Bayesian estimation of variability in adipose tissue blood flow in man by physiologically based pharmacokinetic modeling of inhalation exposure to toluene. Toxicology 157(3):177–193
12. Gueorguieva I, Aarons L, Rowland M (2006) Diazepam pharamacokinetics from preclinical to phase I using a Bayesian population physiologically based pharmacokinetic model with informative prior distributions in WinBUGS. J Pharmacokinet Pharmacodyn 33(5):571–594. doi:10.1007/s10928-006-9023-3
13. Nestorov I (2007) Whole-body physiologically based pharmacokinetic models. Expert Opin Drug Metab Toxicol 3(2):235–249. doi:10.1517/17425255.3.2.235
14. Willmann S, Hohn K, Edginton A, Sevestre M, Solodenko J, Weiss W, Lippert J, Schmitt W (2007) Development of a physiology-based whole-body population model for assessing the influence of individual variability on the pharmacokinetics of drugs. J Pharmacokinet Pharmacodyn 34(3):401–431. doi:10.1007/s10928-007-9053-5
15. Gomez-Mancilla B, Berry-Kravis E, Hagerman R, von Raison F, Apostol G, Ufer M, Gasparini F, Jacquemont S (2014) Development of mavoglurant and its potential for the treatment of fragile X syndrome. Expert Opin Investig Drugs 23(1):125–134. doi:10.1517/13543784.2014.857400
16. Jakab A, Winter S, Raccuglia M, Picard F, Dumitras S, Woessner R, Mistry S, Chudasama J, Guttikar S, Kretz O (2013) Validation of an LC-MS/MS method for the quantitative determination of mavoglurant (AFQ056) in human plasma. Anal Bioanal Chem 405(1):215–223. doi:10.1007/s00216-012-6456-y
17. Yu LX, Lipka E, Crison JR, Amidon GL (1996) Transport approaches to the biopharmaceutical design of oral drug delivery systems: prediction of intestinal absorption. Adv Drug Deliv Rev 19(3):359–376
18. Hintz RJ, Johnson KC (1989) The effect of particle size distribution on dissolution rate and oral absorption. Int J Pharm 51(9–17):9–17
19. Takano R, Sugano K, Higashida A, Hayashi Y, Machida M, Aso Y, Yamashita S (2006) Oral absorption of poorly water-soluble drugs: computer simulation of fraction absorbed in humans from a miniscale dissolution test. Pharm Res 23(6):1144–1156. doi:10.1007/s11095-006-0162-4
20. Nestorov I (2001) Modelling and simulation of variability and uncertainty in toxicokinetics and pharmacokinetics. Toxicol Lett 120(1–3):411–420
21. Howgate EM, Rowland Yeo K, Proctor NJ, Tucker GT, Rostami-Hodjegan A (2006) Prediction of in vivo drug clearance from in vitro data. I: impact of inter-individual variability. Xenobiotica 36(6):473–497. doi:10.1080/00498250600683197
22. Fieller EC (1954) Some problems in interval estimation. J R Stat Soc B 16(2):175–185
23. Jansson R, Bredberg U, Ashton M (2008) Prediction of drug tissue to plasma concentration ratios using a measured volume of distribution in combination with lipophilicity. J Pharm Sci 97(6):2324–2339. doi:10.1002/jps.21130
24. Boeckmann AJ, Sheiner LB, Beal SL (2013) NONMEM users guide—part VIII. ICON Development Solutions, Hanover
25. Martins JRRA, Sturdza P, Alonson JJ (2003) The complex-step derivative approximation. ACM Trans Math Softw 29:245–262
26. Yetter RA, Dryer FL, Rabitz H (1985) Some interpretive aspects of elementary sensitivity gradients in combustion kinetics modeling. Combust Flame 59:107–133
27. Gelman A, Rubin DB (1992) Inference from iterative simulation using multiple sequences. Stat Sci 7(4):457–472. doi:10.2307/2246093
28. Best NG, Cowles MK, Vines SK (1995) CODA manual version 0.30. MRC Biostatistics Uni, Cambridge

29. Oberle RL, Chen TS, Lloyd C, Barnett JL, Owyang C, Meyer J, Amidon GL (1990) The influence of the interdigestive migrating myoelectric complex on the gastric emptying of liquids. Gastroenterology 99(5):1275–1282
30. Yu LX, Amidon GL (1998) Saturable small intestinal drug absorption in humans: modeling and interpretation of cefatrizine data. Eur J Pharm Biopharm 45(2):199–203
31. Tsamandouras N, Wendling T, Rostami-Hodjegan A, Galetin A, Aarons L (2015) Incorporation of stochastic variability in mechanistic population pharmacokinetic models: handling the physiological constraints using normal transformations. J Pharmacokinet Pharmacodyn. doi:10.1007/s10928-015-9418-0
32. Schiller C, Frohlich CP, Giessmann T, Siegmund W, Monnikes H, Hosten N, Weitschies W (2005) Intestinal fluid volumes and transit of dosage forms as assessed by magnetic resonance imaging. Aliment Pharmacol Ther 22(10):971–979. doi:10.1111/j.1365-2036.2005.02683.x
33. Lennernas H (2014) Human in vivo regional intestinal permeability: importance for pharmaceutical drug development. Mol Pharm 11(1):12–23. doi:10.1021/mp4003392
34. Valentin J (2002) Guide for the practical application of the ICRP Human Respiratory Tract Model. A report of ICRP supporting guidance 3: approved by ICRP committee 2 in October 2000. Ann ICRP 32(1–2):13–306
35. Matheson PJ, Wilson MA, Garrison RN (2000) Regulation of intestinal blood flow. J Surg Res 93(1):182–196. doi:10.1006/jsre.2000.5862
36. Paine MF, Khalighi M, Fisher JM, Shen DD, Kunze KL, Marsh CL, Perkins JD, Thummel KE (1997) Characterization of interintestinal and intraintestinal variations in human CYP3A-dependent metabolism. J Pharm Exp Ther 283(3):1552–1562
37. Sun D, Lennernas H, Welage LS, Barnett JL, Landowski CP, Foster D, Fleisher D, Lee KD, Amidon GL (2002) Comparison of human duodenum and Caco-2 gene expression profiles for 12,000 gene sequences tags and correlation with permeability of 26 drugs. Pharm Res 19(10):1400–1416
38. Sjogren E, Abrahamsson B, Augustijns P, Becker D, Bolger MB, Brewster M, Brouwers J, Flanagan T, Harwood M, Heinen C, Holm R, Juretschke HP, Kubbinga M, Lindahl A, Lukacova V, Munster U, Neuhoff S, Nguyen MA, Peer A, Reppas C, Hodjegan AR, Tannergren C, Weitschies W, Wilson C, Zane P, Lennernas H, Langguth P (2014) In vivo methods for drug absorption - comparative physiologies, model selection, correlations with in vitro methods (IVIVC), and applications for formulation/API/excipient characterization including food effects. Eur J Pharm Sci 57:99–151. doi:10.1016/j.ejps.2014.02.010
39. Zhao P, Ragueneau-Majlessi I, Zhang L, Strong JM, Reynolds KS, Levy RH, Thummel KE, Huang SM (2009) Quantitative evaluation of pharmacokinetic inhibition of CYP3A substrates by ketoconazole: a simulation study. J Clin Pharmacol 49(3):351–359. doi:10.1177/0091270008331196
40. Walsky RL, Gaman EA, Obach RS (2005) Examination of 209 drugs for inhibition of cytochrome P450 2C8. J Clin Pharmacol 45(1):68–78. doi:10.1177/0091270004270642
41. Stresser DM, Broudy MI, Ho T, Cargill CE, Blanchard AP, Sharma R, Dandeneau AA, Goodwin JJ, Turner SD, Erve JC, Patten CJ, Dehal SS, Crespi CL (2004) Highly selective inhibition of human CYP3Aa in vitro by azamulin and evidence that inhibition is irreversible. Drug Metab Dispos 32(1):105–112. doi:10.1124/dmd.32.1.105
42. Rowland Yeo K, Jamei M, Yang J, Tucker GT, Rostami-Hodjegan A (2010) Physiologically based mechanistic modelling to predict complex drug–drug interactions involving simultaneous competitive and time-dependent enzyme inhibition by parent compound and its metabolite in both liver and gut—the effect of diltiazem on the time-course of exposure to triazolam. Eur J Pharm Sci 39(5):298–309. doi:10.1016/j.ejps.2009.12.002
43. Johnson TN, Rostami-Hodjegan A, Tucker GT (2006) Prediction of the clearance of eleven drugs and associated variability in neonates, infants and children. Clin Pharmacokinet 45(9):931–956. doi:10.2165/00003088-200645090-00005
44. Edginton AN, Schmitt W, Willmann S (2006) Development and evaluation of a generic physiologically based pharmacokinetic model for children. Clin Pharmacokinet 45(10):1013–1034. doi:10.2165/00003088-200645100-00005
45. Edginton AN, Schmitt W, Voith B, Willmann S (2006) A mechanistic approach for the scaling of clearance in children. Clin Pharmacokinet 45(7):683–704. doi:10.2165/00003088-200645070-00004
46. ICRP (1975) Report of the task group on reference man. ICRP Publication 23, Pergamon Press, Oxford
47. Dokoumetzidis A, Aarons L (2009) A method for robust model order reduction in pharmacokinetics. J Pharmacokinet Pharmacodyn 36(6):613–628. doi:10.1007/s10928-009-9141-9
48. Jorgensen AL, FitzGerald RJ, Oyee J, Pirmohamed M, Williamson PR (2012) Influence of CYP2C9 and VKORC1 on patient response to warfarin: a systematic review and meta-analysis. PLoS One 7(8):e44064. doi:10.1371/journal.pone.0044064
49. Wang J, Flanagan DR (1999) General solution for diffusion-controlled dissolution of spherical particles. 1. Theory. J Pharm Sci 88(7):731–738. doi:10.1021/js980236p
50. Wang J, Flanagan DR (2002) General solution for diffusion-controlled dissolution of spherical particles. 2. Evaluation of experimental data. J Pharm Sci 91(2):534–542
51. Berg D, Godau J, Trenkwalder C, Eggert K, Csoti I, Storch A, Huber H, Morelli-Canelo M, Stamelou M, Ries V, Wolz M, Schneider C, Di Paolo T, Gasparini F, Hariry S, Vandemeulebroecke M, Abi-Saab W, Cooke K, Johns D, Gomez-Mancilla B (2011) AFQ056 treatment of levodopa-induced dyskinesias: results of 2 randomized controlled trials. Mov Disord 26(7):1243–1250. doi:10.1002/mds.23616
52. Stocchi F, Rascol O, Destee A, Hattori N, Hauser RA, Lang AE, Poewe W, Stacy M, Tolosa E, Gao H, Nagel J, Merschhemke M, Graf A, Kenney C, Trenkwalder C (2013) AFQ056 in Parkinson patients with levodopa-induced dyskinesia: 13-week, randomized, dose-finding study. Mov Disord 28(13):1838–1846. doi:10.1002/mds.25561
53. Brown RP, Delp MD, Lindstedt SL, Rhomberg LR, Beliles RP (1997) Physiological parameter values for physiologically based pharmacokinetic models. Toxicol Ind Health 13(4):407–484
54. Yang J, Jamei M, Yeo KR, Tucker GT, Rostami-Hodjegan A (2007) Prediction of intestinal first-pass drug metabolism. Curr Drug Metab 8(7):676–684